Electronic Supplementary Material (ESI) for Journal of Materials Chemistry C.

Supporting Information

Crystal Growth, Structural and Electronic Characterizations of Zero-Dimensional Metal Halide (TEP)$InBr_4$ Single Crystals for X-Ray Detection

Zheng Zhang[a], Tony M. Pugliano[a], Da Cao[b], Doup Kim[b], Roshan S. Annam[c], Dilruba A. Popy[a], Tamanna Pinky[a], Ge Yang[b], Jivtesh Garg[c], Mario F. Borunda[d], Bayram Saparov[a]*

[a]Department of Chemistry and Biochemistry, University of Oklahoma, Norman, OK 73019
[b]Department of Nuclear Engineering, North Carolina State University, Raleigh, NC 27607
[c]School of Aerospace and Mechanical Engineering, University of Oklahoma, Norman, OK 73019
[d]Department of Physics, Oklahoma State University, Stillwater, OK 74078

*Author to whom correspondence should be addressed: saparov@ou.edu

Table S1. Atomic coordinates and equivalent isotropic displacement parameters (U_{eq}[a]) for (TEP)$InBr_4$.

Atom	*x*	*y*	*z*	U_{eq}, Å^2
In(1A)	0.66864(5)	0.67286(6)	0.98739(7)	0.0221(3)
In(1B)	0.66032(6)	0.66394(5)	0.49543(7)	0.0218(3)
In(1C)	0.666667	0.333333	0.50106(16)	0.0219(5)
In(1D)	0.666667	0.333333	0.00136(17)	0.0217(5)
In(1E)	1.000000	1.000000	1.00492(15)	0.0206(4)
Br(1A)	0.60954(8)	0.56345(8)	1.03155(13)	0.0274(4)
Br(2A)	0.76684(8)	0.72657(8)	1.07684(13)	0.0266(4)
Br(3A)	0.60799(7)	0.72271(8)	1.02326(13)	0.0281(4)
Br(4A)	0.69275(8)	0.67935(8)	0.80943(12)	0.0293(3)
Br(1B)	0.72169(8)	0.77514(8)	0.52577(16)	0.0270(4)
Br(2B)	0.55817(7)	0.62568(8)	0.56999(14)	0.0288(3)
Br(3B)	0.70914(8)	0.60925(7)	0.56763(14)	0.0283(4)
Br(4B)	0.64916(8)	0.64371(8)	0.31592(12)	0.0339(4)
Br(1C)	0.73569(8)	0.43849(8)	0.56020(13)	0.0314(4)
Br(2C)	0.666667	0.333333	0.3184(3)	0.0282(7)
Br(1D)	0.59658(8)	0.22824(8)	0.06006(13)	0.0275(3)
Br(2D)	0.666667	0.333333	-0.1811(3)	0.0254(7)
Br(1E)	1.10433(8)	1.07266(8)	1.06429(13)	0.0272(3)
Br(2E)	1.000000	1.000000	0.8230(2)	0.0271(7)
P(1F)	0.8897(2)	0.43912(18)	0.7427(3)	0.0189(9)
P(1G)	0.5582(2)	0.77965(18)	0.7371(3)	0.0203(9)
P(1H)	1.10578(18)	1.22425(19)	1.2444(3)	0.0184(9)
C(1F)	0.8774(8)	0.4717(9)	0.8493(13)	0.034(4)
C(2F)	0.8255(8)	0.4843(9)	0.8428(13)	0.033(4)
C(3F)	0.8976(7)	0.4851(7)	0.6394(11)	0.027(3)
C(4F)	0.9057(12)	0.4607(9)	0.5406(14)	0.045(6)
C(5F)	0.8269(7)	0.3645(7)	0.7228(11)	0.025(3)
C(6F)	0.8182(10)	0.3172(9)	0.8012(12)	0.041(5)
C(7F)	0.9568(7)	0.4344(8)	0.7586(12)	0.029(4)
C(8F)	1.0155(9)	0.4973(10)	0.7755(15)	0.044(6)
C(1G)	0.5691(7)	0.8295(7)	0.6360(11)	0.028(3)

C(2G)	0.5813(9)	0.8078(9)	0.5372(12)	0.034(4)
C(3G)	0.4929(7)	0.7082(7)	0.7154(11)	0.027(3)
C(4G)	0.4798(9)	0.6612(10)	0.7954(13)	0.037(5)
C(5G)	0.6235(8)	0.7716(8)	0.7521(12)	0.031(4)
C(6G)	0.6812(9)	0.8301(9)	0.7738(15)	0.041(5)
C(7G)	0.5476(8)	0.8131(9)	0.8463(11)	0.036(4)
C(8G)	0.4957(8)	0.8259(8)	0.8390(13)	0.038(5)
C(1H)	1.1371(8)	1.2137(8)	1.3556(10)	0.025(4)
C(2H)	1.1504(9)	1.1633(9)	1.3532(12)	0.032(4)
C(3H)	1.0978(7)	1.2894(8)	1.2551(12)	0.024(3)
C(4H)	1.1573(8)	1.3495(9)	1.2743(13)	0.034(5)
C(5H)	1.0327(7)	1.1588(8)	1.2203(11)	0.027(4)
C(6H)	0.9858(8)	1.1493(9)	1.2942(12)	0.032(4)
C(7H)	1.1557(8)	1.2339(8)	1.1460(10)	0.025(3)
C(8H)	1.1336(9)	1.2424(9)	1.0470(11)	0.028(4)

[a] U_{eq} is defined as one third of the trace of the orthogonalized U_{ij} tensor.

Table S2. Selected bond distances and angles within the $[InBr_4]^-$ tetrahedra in $(TEP)InBr_4$.

Atom pair	Distance (Å)	Label	Angle (°)
In(1A)-Br(3A)	2.499(2)	Br(3A)-In(1A)-Br(1A)	109.93(7)
In(1A)-Br(1A)	2.499(2)	Br(3A)-In(1A)-Br(2A)	109.38(7)
In(1A)-Br(2A)	2.500(2)	Br(1A)-In(1A)-Br(2A)	112.00(7)
In(1A)-Br(4A)	2.505(2)	Br(3A)-In(1A)-Br(4A)	110.69(7)
In(1B)-Br(3B)	2.498(2)	Br(1A)-In(1A)-Br(4A)	107.56(7)
In(1B)-Br(1B)	2.501(2)	Br(2A)-In(1A)-Br(4A)	107.25(7)
In(1B)-Br(2B)	2.504(2)	Br(3B)-In(1B)-Br(1B)	111.41(7)
In(1B)-Br(4B)	2.505(2)	Br(3B)-In(1B)-Br(2B)	109.54(7)
In(1C)-Br(1C)	2.5011(19)	Br(1B)-In(1B)-Br(2B)	108.36(8)
In(1C)-Br(1C)	2.5011(19)	Br(3B)-In(1B)-Br(4B)	108.18(7)
In(1C)-Br(1C)	2.5011(19)	Br(1B)-In(1B)-Br(4B)	109.91(8)
In(1C)-Br(2C)	2.508(5)	Br(2B)-In(1B)-Br(4B)	109.43(8)
In(1D)-Br(1D)	2.5027(19)	Br(1C)-In(1C)-Br(1C)	110.00(7)
In(1D)-Br(1D)	2.5028(19)	Br(1C)-In(1C)-Br(1C)	110.00(6)
In(1D)-Br(1D)	2.5028(19)	Br(1C)-In(1C)-Br(1C)	110.00(7)
In(1D)-Br(2D)	2.505(5)	Br(1C)-In(1C)-Br(2C)	108.94(7)
In(1E)-Br(2E)	2.498(4)	Br(1C)-In(1C)-Br(2C)	108.94(7)
In(1E)-Br(1E)	2.5046(19)	Br(1C)-In(1C)-Br(2C)	108.94(7)
In(1E)-Br(1E)	2.5047(19)	Br(1D)-In(1D)-Br(1D)	110.15(6)
In(1E)-Br(1E)	2.5048(19)	Br(1D)-In(1D)-Br(1D)	110.15(6)
		Br(1D)-In(1D)-Br(1D)	110.15(6)
		Br(1D)-In(1D)-Br(2D)	108.78(6)
		Br(1D)-In(1D)-Br(2D)	108.78(6)
		Br(1D)-In(1D)-Br(2D)	108.78(6)
		Br(2E)-In(1E)-Br(1E)	108.99(6)
		Br(2E)-In(1E)-Br(1E)	108.99(6)
		Br(1E)-In(1E)-Br(1E)	109.95(6)
		Br(2E)-In(1E)-Br(1E)	108.99(6)
		Br(1E)-In(1E)-Br(1E)	109.94(6)
		Br(1E)-In(1E)-Br(1E)	109.95(6)

1. Powder X-ray diffraction measurements

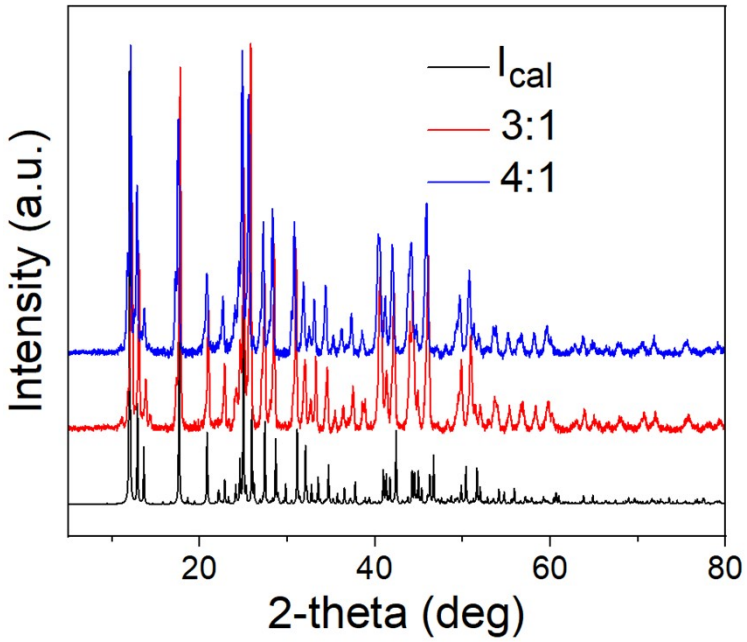

Figure S1. Measured powder X-ray diffraction pattern using the obtained synthesized products from molar ratio 3:1 ($TEPBr:InBr_3$) and 4:1 solution. I_{cal} is the calculated theoretical pattern given by single crystal X-ray diffraction measurement for $(TEP)InBr_4$.

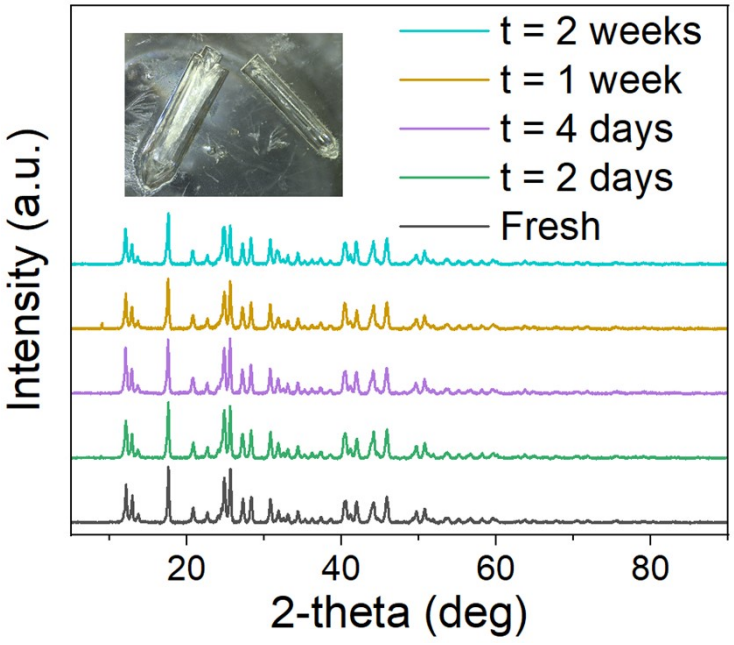

Figure S2. A comparison of PXRD patterns measured for a fresh $(TEP)InBr_4$ sample and the same sample after air exposure for days. Inset is a photograph of the as-grown $(TEP)InBr_4$ single crystals.

2. Frequency domain thermoreflectance data for $(TEP)InBr_4$

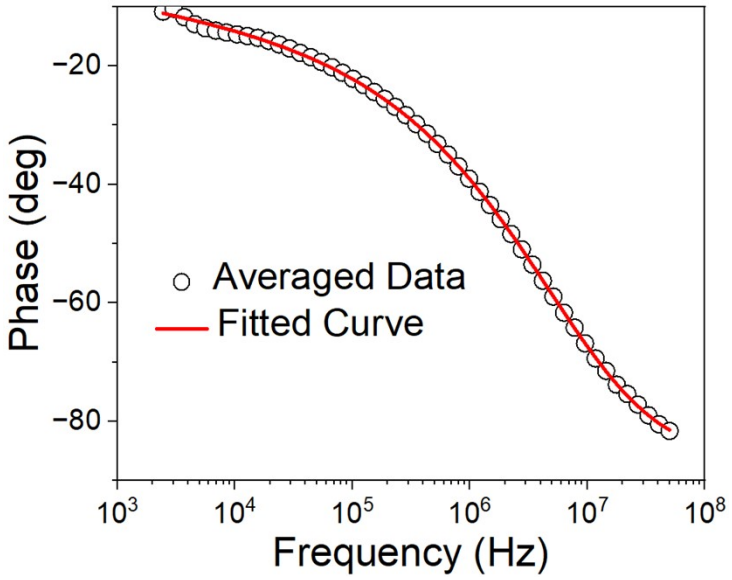

Figure S3. Measured phase lag from FDTR measurements and the fitted curve using 2D diffusion thermal model. Note that due to the uneven crystal surface, 15 sampling points on the crystal surface were selected and data were then averaged.

3. Sample-to-sample variations in resistivity

Table S3. Resistivity measured for the selected four $(TEP)InBr_4$ single crystal samples.

Sample	Metal Contact	Electrode Area (cm^2)	Thickness (cm)	Resistivity ($\Omega \cdot cm$)
1	Ag	0.25×0.1	0.1	1.72×10^{13}
2	Ag	0.15×0.1	0.1	6.86×10^{12}
3	Ag	0.22×0.06	0.05	1.79×10^{13}
4	Ag	0.22×0.1	0.1	1.69×10^{13}

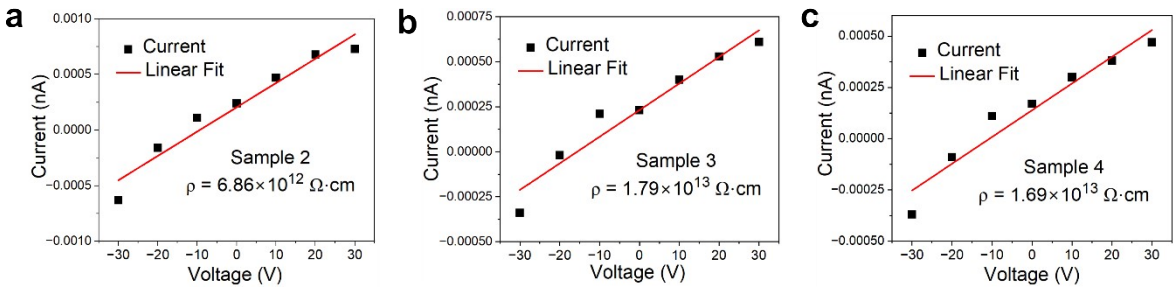

Figure S4. Variation in semiconductor resistivity values measured for different $(TEP)InBr_4$ single crystals: (a) sample 2, (b) sample 3, and (c) sample 4.

4. Calculations of the rise and decay times

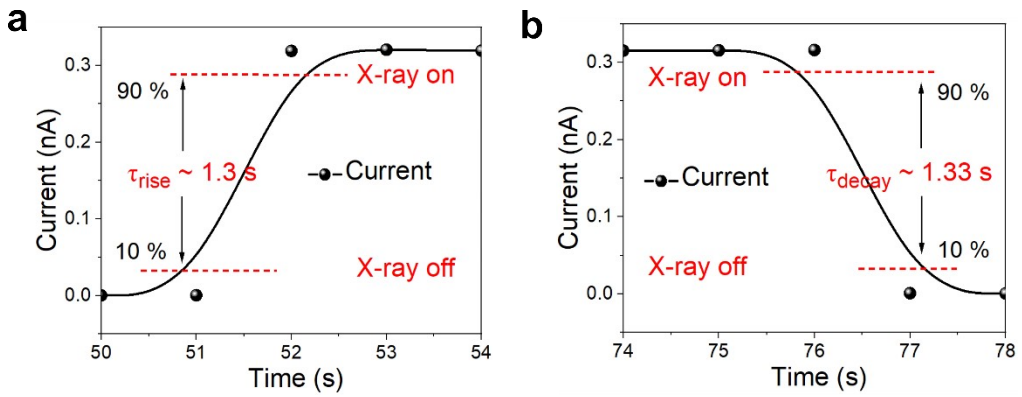

Figure S5. Calculation of the (a) rise time τ_{rise}, and (b) decay time τ_{decay} using the time interval between 10% and 90% of the current amplitude.

5. The lowest detectable dose rate determination

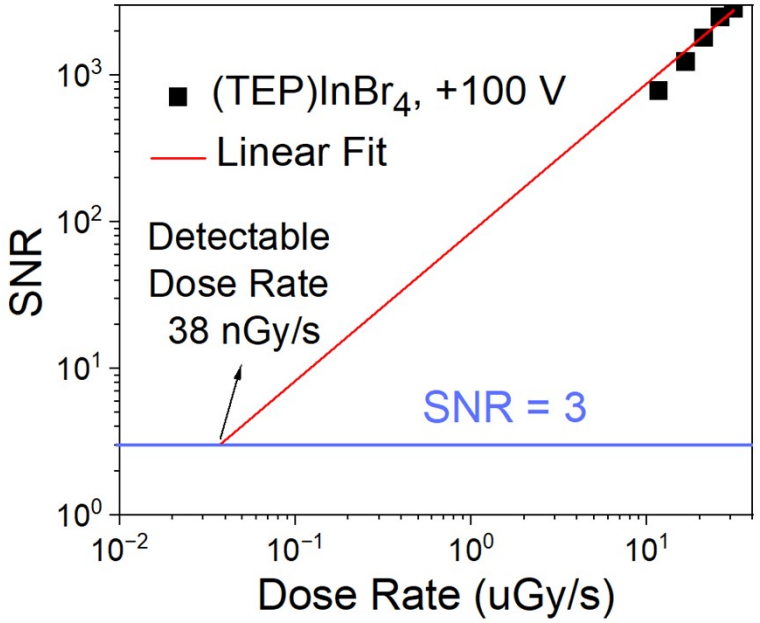

Figure S6. SNR vs. dose rate plot at +100 V elongated to the intersection with the line SNR=3 to determine the lowest detectable dose rate.

6. Summary of the X-ray detector performance characteristics

Table S4. A comparison of the X-ray detector performance characteristics using (TEP)$InBr_4$ single crystal with other reported metal halides.

Metal Halide	Resistivity (Ω·cm)	mu-tau Product (cm^2/V)	Sensitivity ($uCGy^{-1}cm^{-2}$)	Lowest Detectable Dose Rate (nGy/s)	Reference
3D $Cs_2AgBiBr_6$	2.59×10^{9}	3.75×10^{-3}	105 (at E = 25 V/mm)	59.7	1
2D $BDAPbI_4$	-	4.43×10^{-4}	242 (at E = 310 V/mm)	430	2
2D $(PMA)_2PbI_4$	-	1.46×10^{-3}	283 (at bias 50 V)	2130	3
1D $(DMEDA)BiI_5$	-	-	72.5 (at E = 494 V/mm)	-	4
0D $MA_3Bi_2I_9$	10^{10}-10^{11}	10^{-3}	10620 (out-of-plane) ~212.4 (in-plane) (at bias 120 V)	0.62	5
0D $(DPA)_2BiI_9$	5.0×10^{10}	10^{-4}-10^{-3}	20570 (at bias 120 V)	0.98	6
0D (TEP)$InBr_4$	1.72×10^{13}	2.07×10^{-5}	569.85 (at E = 100 V/mm)	38	this work

7. Current-voltage measurements under X-ray radiation

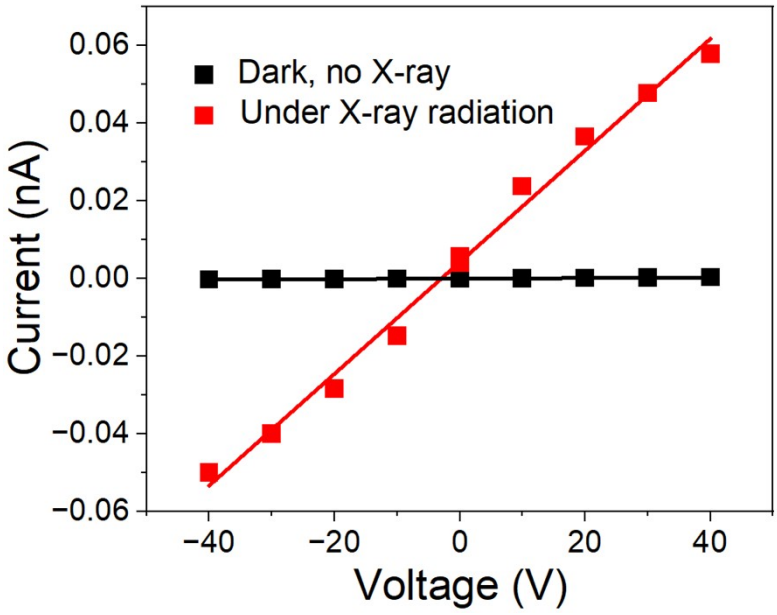

Figure S7. Comparison of the current-voltage (I-V) curves obtained for (TEP)$InBr_4$ single crystals in dark (no X-ray irradiation) and under continuous X-ray radiation from a tungsten source.

8. Zoom-in plot of the band structure

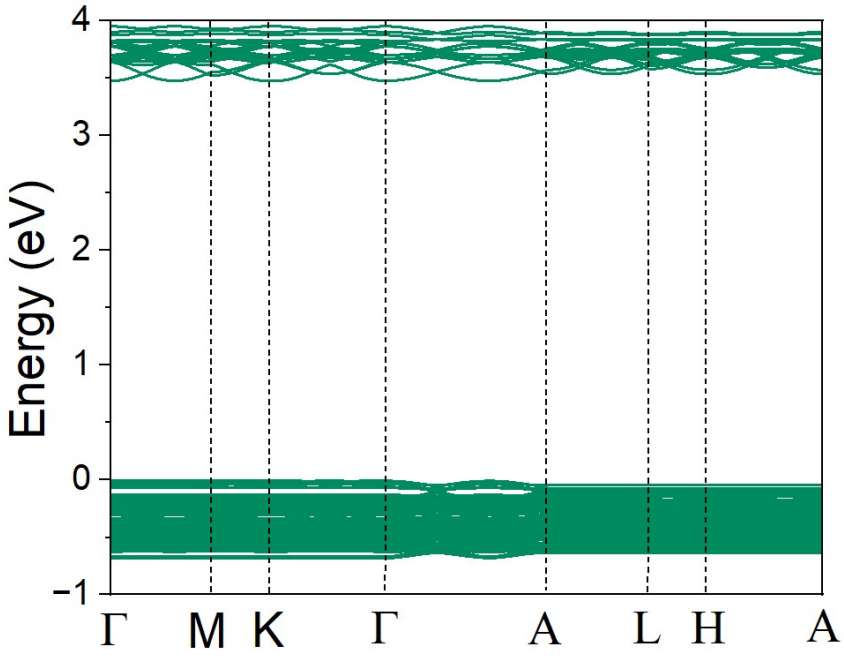

Figure S8. Zoom-in plot of the electronic bandgap structure of (TEP)$InBr_4$.

References

1. Pan, W.; Wu, H.; Luo, J.; Deng, Z.; Ge, C.; Chen, C.; Jiang, X.; Yin, W. J.; Niu, G.; Zhu, L.; Yin, L.; Zhou, Y.; Xie, Q.; Ke, X.; Sui, M.; Tang, J. Cs2AgBiBr6 Single-Crystal X-Ray Detectors with a Low Detection Limit. *Nat. Photonics* **2017**, *11* (11), 726–732.
2. Shen, Y.; Liu, Y.; Ye, H.; Zheng, Y.; Wei, Q.; Xia, Y.; Chen, Y.; Zhao, K.; Huang, W.; Liu, S. Centimeter-Sized Single Crystal of Two-Dimensional Halide Perovskites Incorporating Straight-Chain Symmetric Diammonium Ion for X-Ray Detection. *Angew. Chemie - Int. Ed.* **2020**, *59* (35), 14896–14902.
3. Qian, C. X.; Wang, M. Z.; Lu, S. S.; Feng, H. J. Fabrication of 2D Perovskite (PMA)2PbI4crystal and Cu Ion Implantation Improved x-Ray Detector. *Appl. Phys. Lett.* **2022**, *120* (1).
4. Yao, L.; Niu, G.; Yin, L.; Du, X.; Lin, Y.; Den, X.; Zhang, J.; Tang, J. Bismuth Halide Perovskite Derivatives for Direct X-Ray Detection. *J. Mater. Chem. C* **2020**, *8* (4), 1239–1243.
5. Zheng, X.; Zhao, W.; Wang, P.; Tan, H.; Saidaminov, M. I.; Tie, S.; Chen, L.; Peng, Y.; Long, J.; Zhang, W. H. Ultrasensitive and Stable X-Ray Detection Using Zero-Dimensional Lead-Free Perovskites. *J. Energy Chem.* **2020**, *49*, 299–306.
6. Wang, Y.; Zhang, S.; Wang, Y.; Yan, J.; Yao, X.; Xu, M.; Lei, X. W.; Lin, G.; Yue, C. Y. 0D Triiodide Hybrid Halide Perovskite for X-Ray Detection. *Chem. Commun.* **2023**, *59* (60), 9239–9242.